Shock Waves (2021) 31:133–140
https://doi.org/10.1007/s00193-021-01007-9

ORIGINAL ARTICLE

Evolution of heat transfer at the stagnation point during the detached bow shock establishment

Q. Wang[1] · J. P. Li[1] · K. Luo[1,2] · J. W. Li[1] · W. Zhao[1,2]

Received: 1 February 2019 / Revised: 17 June 2019 / Accepted: 8 March 2021 / Published online: 2 April 2021

Abstract
The diffraction of a shock wave over a stationary body is a problem of interest associated with the starting of shock tubes and expansion tubes which are well suited to studies of hypersonic flows. However, these facilities are characterized by very short test times. The transient parameters during the establishment of the detached bow shock in such impulsive facilities are important for both data processing and experimental design. In the present study, numerical simulations are conducted to investigate the diffraction of a normal shock wave over a sphere and the subsequent transient phenomena in a viscous perfect-gas flow field. The incident shock Mach number ranges from 3 to 5 with a specific heat ratio of 1.4. Based on the theoretical description of the reflected shock position during bow shock formation, approximate solutions for the time histories of the stagnation-point heat flux are also derived. The analytical and numerical results agree well. The results show that the stagnation-point pressure and heat flux approach their steady-state values much more rapidly than the shock detachment distance does.

Keywords Hypersonic · Aerodynamic heating · Detached bow shock · Shock tube/expansion tube

1 Introduction

The development of new aerospace vehicles calls for reliable aeroheating prediction methods for hypersonic flows. In general, the local convective heat transfer rate is maximal at the stagnation point (if the boundary layer remains laminar), which is downstream from the normal portion of the bow shock wave. The same point is often used as the denominator in non-dimensional correlations of convective heat transfer distributions [1]. As a consequence, any uncertainty in this value may propagate to the final quantities of interest and contribute to a reduction of overall measurement accuracy. Therefore, defining the flow field in the stagnation region and the heat transfer at the stagnation point is a problem of both theoretical and practical interest [2].

Due to the high cost of flight tests, most aerodynamic-heating experiments are performed in ground impulsive facilities, which can simulate the required aerothermal environment at low cost of operation. Hypersonic flow about a model that is mounted in a shock tube or expansion tube is initiated by causing a normal shock wave to travel down the tube and past the model. When the shock strikes the model, it diffracts over it and a shock layer forms ahead of the model. This shock layer adjusts with time until a steady flow is established. Several studies investigated the flow-establishment time for model experiments in hypersonic facilities with short test times [3–8]. Most of them focused on evaluating the length of flow-establishment time or using high-speed optical recorders to obtain the stand-off distance and the speed of bow shock movement. Furthermore, approximate expressions for the time history of the shock detachment distance are utilized for blunt bodies that are washed by a normal shock. Moreover, Moran and Moorhem [5] and Barnwell [6] predicted the pressure distribution on smooth blunt bodies for as long as possible after the arrival of the incident shock. Unfortunately, the heat transfer distributions during the establishment of the detached bow shock have rarely been

Communicated by K. Hannemann.

✉ J. P. Li
lijinping@imech.ac.cn

[1] State Key Laboratory of High Temperature Gas Dynamics, Institute of Mechanics, Chinese Academy of Sciences, No. 15 Beisihuanxi Road, Beijing 100190, China

[2] School of Engineering Science, University of Chinese Academy of Sciences, No. 19 Yuquan Road, Beijing 100049, China

reported so far. Li et al. [9] briefly described the jumps in the heat flux at the stagnation point after the arrival of the incident shock in a detonation shock tube and pointed out that it takes a specific time for the heat flux to gradually decrease to a final constant value. Collen et al. [10] presented the measured heat flux and reflected shock speed/position during shock establishment. They also discussed the overshoot of heat flux at the initial stage after the shock arrival. During shock establishment, significantly higher gas temperatures are present as the incoming gas stagnates completely on the front surface of the probe, resulting in a reflected shock traveling upstream. This shock quickly weakens, causing a corresponding reduction in the post-shock pressure and heat transfer. However, these results were not discussed and quantified in detail. In addition, hypersonic facilities come at the expense of test time; for example, the X2 expansion tube has a test time as short as 50–500 μs [11,12]. Miller and Moore showed that the time required for the stagnation-point heat flux to approach an essentially constant value was about 80 μs [7]. Therefore, there is always a question as to whether or not the test times are sufficient to allow the establishment of certain types of steady flows over aerodynamic models. If available test times are not sufficiently long to obtain a steady-state flow over aerodynamic models, the experimental data of these facilities are not reliable for an accurate representation of simulated flow fields. To properly design heat transfer measurement experiments in impulsive facilities and to interpret data from such facilities, it remains necessary to understand how the flow and heat transfer approaches the steady-state condition by knowing the transient flow field. Moreover, although the contributions of computational fluid dynamics (CFD) have demonstrated significant progress over the past two decades, the simulation of aerodynamic heating is still full of complexities [13,14]. An analytical approach may provide a more intuitive and accessible prediction.

The primary goal of the present study was to examine the transient heat flux at the stagnation point during detached bow shock establishment. Both CFD and theoretical analysis were conducted, and different incident shock Mach numbers were considered. Heat convection or heat conduction was employed to represent the stagnation-point heat transfer in the theoretical analysis, and approximate analytical solutions were obtained. The analytical solutions were validated by numerical results, and the corresponding phenomena were discussed in detail. The related mechanisms were investigated accordingly in the effort to provide theoretical guidance for both data processing and experimental design of aerodynamic-heating experiments in short-test-time impulsive facilities, such as shock tubes or expansion tubes.

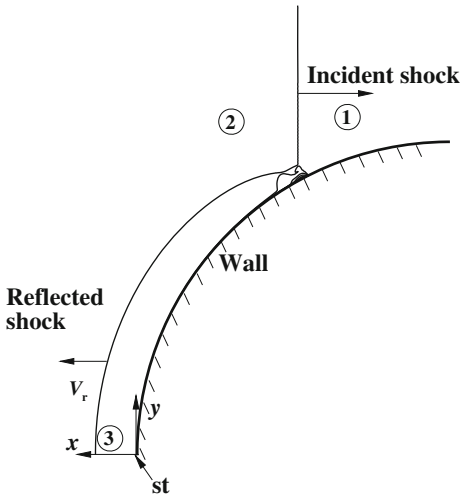

Fig. 1 Shock reflection at a sphere; numbers are used to identify flow regions defined by the incident and reflected shock waves and the wall

2 Simulation methodology

The considered problem is the diffraction of an incident shock wave over a sphere, as illustrated in Fig. 1. A strong shock moving in a gas at rest and sweeping over a blunt body is reflected at the stagnation point $x = 0$. The reflected shock running upstream is decelerated and, after a specific formation time, establishes as a steady bow shock wave at the distance $x = \Delta$, where Δ represents the steady bow shock stand-off distance. The phenomenon under consideration is the unsteady flow in the shock layer ahead of the body after shock impingement and before the establishment of steady flow.

Since high-accuracy heat transfer measurements remain largely elusive due to their excessive complexity, numerical simulations were conducted to better understand the unsteady evolutionary process during the movement of the shock wave. The following governing equations were employed (the axisymmetric, unsteady, compressible Navier–Stokes equations assuming laminar flow):

$$\frac{\partial U}{\partial t} + \frac{\partial F}{\partial x} + \frac{\partial G}{\partial y} + H = \frac{\partial F_{\mathrm{v}}}{\partial x} + \frac{\partial G_{\mathrm{v}}}{\partial y} + H_{\mathrm{v}}, \tag{1}$$

$$U = (\rho, \rho u, \rho v, E)^{\mathrm{T}},$$
$$F = (\rho u, \rho u^2 + p, \rho uv, u(E + p))^{\mathrm{T}},$$
$$G = (\rho v, \rho uv, \rho v^2 + p, v(E + p))^{\mathrm{T}},$$
$$F_{\mathrm{v}} = (0, \tau_{xx}, \tau_{xy}, u\tau_{xx} + v\tau_{xy} + q_x)^{\mathrm{T}},$$
$$G_{\mathrm{v}} = (0, \tau_{xy}, \tau_{yy}, u\tau_{xy} + v\tau_{yy} + q_y)^{\mathrm{T}},$$
$$H = \frac{1}{y}(\rho v, \rho uv, \rho v^2 + p, v(E + p))^{\mathrm{T}},$$
$$H_{\mathrm{v}} = \frac{1}{y}(0, \tau_{xy}, \tau_{yy} - \tau_{\theta\theta}, u\tau_{xy} + v\tau_{yy} + q_y)^{\mathrm{T}}, \tag{2}$$

where x and y are the axial and radial coordinates of the physical space; t is time; U is the conservative variable vector; F, G, and H are the inviscid flux vectors; and F_v, G_v, and H_v are the viscous flux vectors. The variables ρ, u, and E are density, velocity, and the total energy per unit volume, respectively. The shear stresses, heat flux, and the state equations are given by the following equations:

$$\tau_{xx} = \frac{2}{3}\mu\left(2\frac{\partial u}{\partial x} - \frac{\partial v}{\partial y}\right), \quad \tau_{yy} = \frac{2}{3}\mu\left(2\frac{\partial v}{\partial y} - \frac{\partial u}{\partial x}\right),$$
$$\tau_{xy} = \mu\left(\frac{\partial u}{\partial y} + \frac{\partial v}{\partial x}\right), \tag{3}$$

$$q_x = -k\frac{\partial T}{\partial x}, \quad q_y = -k\frac{\partial T}{\partial y}, \tag{4}$$

$$E = \frac{p}{\gamma - 1} + \rho\frac{u^2 + v^2}{2}, \quad p = \rho RT. \tag{5}$$

The viscosity coefficient μ in (3) is computed by the Sutherland formula, while the thermal conductivity coefficient k in (4) is derived from the Prandtl number. The definition of other variables can be found in the literature [15].

The governing equations were solved using a finite-difference approach; convective terms were approximated using the AUSMPW+ scheme [16,17], and a central difference method was applied to the viscous terms. Time integration was performed implicitly by applying the LU-SGS algorithm [18]. No-slip and isothermal boundary conditions were specified as the boundary conditions at the wall, and the temperature was set to 293 K.

The validation of the procedure was previously reported in [19]; thus, it is not discussed in detail here. A grid convergence study was conducted for three different grid resolutions (400×320, 500×480, and 800×500 grid points, with the first numbers representing the grid nodes along the axial coordinate; the zones near the wall were incorporated with clustered points). There was a negligible difference in the stagnation-point heat flux normalized by the stable heat flux q_{stable} at $t \to \infty$ for all grids, as shown in Fig. 2. Thus, a mesh size of 500×480 was employed for the present study.

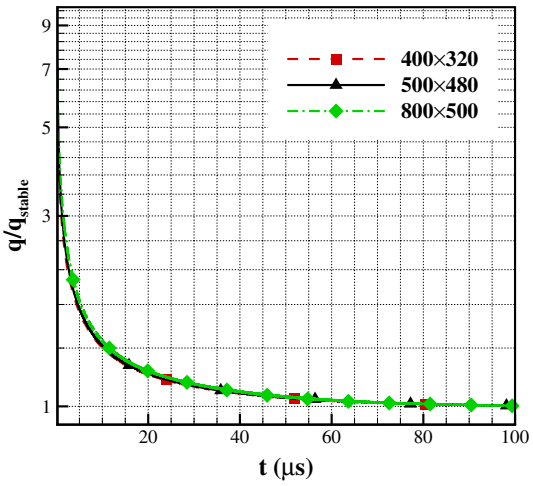

Fig. 2 Stagnation-point heat transfer histories for three grid resolutions with $M_s = 5$, $p_0 = 250$ Pa, $T_0 = 250$ K, $T_w = 293$ K, $\gamma = 1.4$, and $R = 20$ mm

3 Approximate analytical solutions

Although CFD results may provide complete information about the flow field, the simulation of aerodynamic heating still remains complex. This can be addressed via improvement of physical models, numerical schemes, and mesh resolution [14]. In the present paper, an approximate analytical approach was also developed, providing physical insight and a more intuitive and accessible prediction of the stagnation-point heat transfer during the detached bow shock movement. The analytical solutions are compared and validated with the CFD results.

3.1 Bow shock establishment

To identify flow regions defined by the incident and reflected shock waves and the wall, numbers are used as shown in Fig. 1. In the following, subscript 1 represents the properties of the undisturbed flow, subscript 2 represents the properties behind the incident shock, subscript 3 represents the properties immediately after the reflected shock, and subscript st represents the properties at the stagnation point. Furthermore, M_s is the Mach number of the incident shock and $x = x(t)$ is the position of the reflected shock.

Patz [8] developed a single function of the distance–time curve for the reflected shock using the mass-balance method:

$$\frac{d\xi}{d\tau} = 1 - \frac{(1 - \beta\xi)\xi}{1 - \beta}, \tag{6}$$

where β is a free constant. The variables ξ and τ are two dimensionless coordinates defined as follows:

$$\xi = \frac{x}{\Delta}, \quad \tau = \frac{t \cdot V_{r0}}{\Delta}, \tag{7}$$

where $V_r = \frac{dx}{dt}$ is the speed of the reflected shock and t is the time after shock impingement. The approximation of Billing [20] is used to calculate the steady shock stand-off distance in the present study:

$$\frac{\Delta}{R} = 0.143 \cdot e^{3.24/M_2^2}, \tag{8}$$

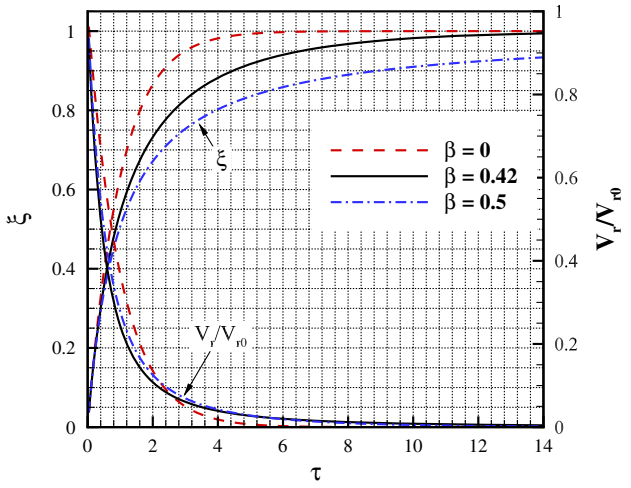

Fig. 3 Shock wave trajectories given by (6)

where R is the radius of the sphere model and M is the flow Mach number (in region 2). It is noted that (6) satisfies the boundary conditions, which are: At $\tau = 0$, $\xi = 0$, $V_r = V_{r0}$, and as $\tau \to \infty$, $\xi = 1$, $V_r = 0$. Subscript 0 represents the initial value at $x = 0$, which could be obtained from the moving shock theory as

$$V_{r0} = \frac{a_1}{\gamma + 1}\left(2(\gamma - 1)M_s + \frac{3 - \gamma}{M_s}\right), \tag{9}$$

where γ is the specific heat ratio (calorically perfect gas is employed in the present study) and a is the sound speed.

In the dimensionless coordinates ξ and τ, as shown in (6), a single function is found to represent the distance–time curve of the reflected shock. It is worth noting that this function is independent from the flow conditions. Researchers used different values of β to obtain the best agreement with their experimental results. Figure 3 shows the variation of the unsteady stand-off distance and reflected shock speed with time calculated from (6), where different values of β are considered.

The Mach number of the reflected shock moving in the relatively static region 2 was defined as $M_r = \frac{V_r + u_2}{a_2}$. Thus, the parameters in region 3 can be obtained from the parameters in region 2:

$$\begin{aligned} \frac{p_3}{p_2} &= 1 + \frac{2\gamma}{\gamma + 1}(M_r^2 - 1), \\ \frac{T_3}{T_2} &= \frac{[2\gamma M_r^2 - (\gamma - 1)][(\gamma - 1)M_r^2 + 2]}{(\gamma + 1)^2 M_r^2}. \end{aligned} \tag{10}$$

Subsequently, the parameters at the stagnation point can be obtained with the relationships of isentropic compression. In other words, all parameters at the stagnation point for the time histories of the detached bow shock establishment can be obtained by the development of a distance–time equation of the shock, e.g., (6).

3.2 Heat transfer at the stagnation point during bow shock establishment

The transient stagnation-point pressure can be easily obtained by the above equations. However, heat flux determination is complicated since it is thought to be a result of a combination of convective heat transfer and heat conduction. At $\tau \to \infty$, a steady bow shock wave is established in front of the model. The heat transfer at the stagnation point is convective and can be obtained by the well-known Fay and Riddell equation [21]:

$$q_{FR} = 0.763 \cdot \mathrm{Pr}^{-0.6}(\rho\mu)_{st}^{0.4}(\rho\mu)_w^{0.1}(h_{st} - h_w)\sqrt{\left(\frac{du}{dy}\right)_{st}}. \tag{11}$$

Since the free stream parameters of region 2 in Fig. 1 are known, it is easy to obtain the stagnation-point heat transfer q_{stable} at $\tau \to \infty$. The following results of the analysis are displayed using the non-dimensional form q/q_{stable}. The results for q/q_{stable} should approach 1 at $\tau \to \infty$.

Figure 3 shows that the reflected shock moves fast at the initial stage and changes slowly after a specific time, which means that the parameters in the boundary layer at the stagnation point change slowly. It is generally accepted that the convective heat transfer is dominant after a specific time of the detached bow shock movement. The Fay and Riddell equation becomes applicable after this moment. Since the parameters at the stagnation line were obtained using the equations in Sect. 3.1, the heat transfer at the stagnation point can also be obtained using (11) for the time histories of the detached bow shock establishment, see q_{FR} in Fig. 4. It shows that q_{FR}/q_{stable} quickly approaches 1.

At $\tau \to 0$, the reflection is regular: It is a moving shock reflection from a rigid wall. It generates an approximate stationary high-temperature gas source, and the heat transfer mechanism at the stagnation point can be assumed to be heat conduction with two materials maintained at a specified initial temperature T_i at the interface ($x = 0$). Therefore, heat conduction is dominant at the initial stage of the detached bow shock movement. The left side is a high-temperature gas and the right side is the solid model, as shown in Fig. 5. If the time period is short, this is similar to two semi-infinite bodies. Then, the heat transfer at the interface can be calculated by solving one-dimensional transient conduction equations for both regions [22], i.e.,

$$q_g = \frac{\sqrt{(\rho c k)_g}}{\sqrt{\pi}}\frac{(T_{st} - T_i)}{\sqrt{t}}, \tag{12}$$

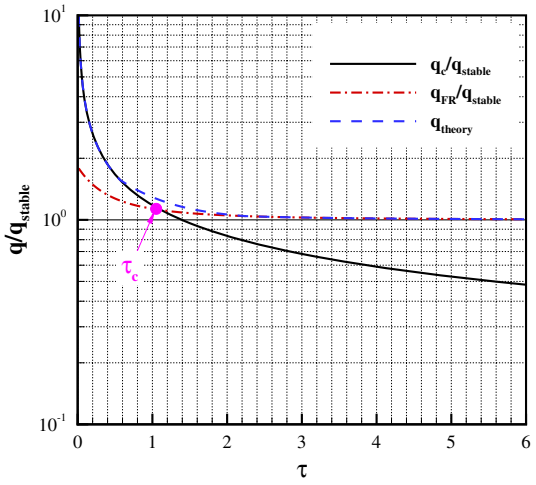

Fig. 4 Stagnation-point heat transfer histories; $M_s = 5$, $p_0 = 250$ Pa, $T_0 = 250$ K, $T_w = 293$ K, $\gamma = 1.4$, and $R = 20$ mm

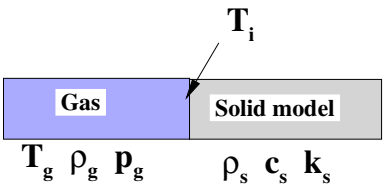

Fig. 5 Schematic diagram of the heat conduction at the initial stage of shock reflection

$$q_s = \frac{\sqrt{(\rho c k)_s}}{\sqrt{\pi}} \frac{(T_i - T_w)}{\sqrt{t}}, \tag{13}$$

where ρ, c, and k are the density, heat capacity, and heat conductivity of the material, respectively. Subscript g represents the properties of high-temperature gas, and subscript s represents the solid sphere model. Since the energy dissipated by the gas is completely absorbed by the sphere model, the heat flux should be the same for them: $q_g = q_s$. Thus, the temperature of the interface can be obtained by:

$$T_i = \frac{T_g\sqrt{(\rho c k)_g} + T_s\sqrt{(\rho c k)_s}}{\sqrt{(\rho c k)_g} + \sqrt{(\rho c k)_s}}. \tag{14}$$

The solid material is treated as stainless steel in the present study since this material is used frequently for test models in impulsive facilities [23]; the corresponding parameters are $\rho_s = 7930$ kg/m^3, $c_s = 500$ J/(kg · K), and $k_s = 17$ W/(m · K). Hence, the heat transfer at the interface can be obtained by (12) and (14) as:

$$q_c = \frac{\sqrt{(\rho c k)_s}}{\sqrt{\pi}} \frac{(T_{r0} - T_i)}{\sqrt{t}} \tag{15}$$

where T_{r0} is the gas temperature right after the reflection of the incident shock ($\tau = 0$). For the gas, the parameters immediately after the reflected shock given by (9) are used. The results using the above equations are shown in Fig. 4 as q_c/q_{stable}.

The heat transfer at the stagnation point has been obtained when τ is either relatively large or small. The intermediate values between the two extremes are unknown and complicated. They result from a combined effect of conduction and convection heat transfer between the fluid and the model. A fitting curve or bridge function is used to predict the heat transfer in this case as follows:

$$q_{theory} = \begin{cases} q_c, & \tau \le 0.5\tau_c \\ 1 + \omega_1 e^{\omega_2 \tau}, & 0.5\tau_c < \tau \le 2\tau_c \\ q_{FR}, & \tau > 2\tau_c \end{cases} \tag{16}$$

where τ_c is defined as the moment when $q_c = q_{FR}$, as shown in Fig. 4. During the period of $\tau \le 0.5\tau_c$, it is heat conduction that plays a leading role in the stagnation-point heat transfer and q_c from (15) is used. For $\tau > 2\tau_c$, convective heat transfer is dominant and q_{FR} from (11) is employed. Within the time period of $0.5\tau_c < \tau \le 2\tau_c$, a simple exponential function is constructed and the constant values of ω_1 and ω_2 are related to the heat transfer values at the moments of $0.5\tau_c$ and $2\tau_c$. The approximate analytical result of (16) is plotted in Fig. 4. Numerical simulations were employed to validate the above analysis. The results shown in Fig. 4 are calculated under the conditions of $M_s = 5$, $p_0 = 250$ Pa, $T_0 = 250$ K, $T_w = 293$ K, $\gamma = 1.4$, and $R = 20$ mm, where $\tau_c = 1.12$ and the corresponding dimensional time is $t = 16.7$ μs.

4 Results and discussion

The diffraction of the incident shock wave by the sphere and the subsequent motion of the reflected shock wave for $M_s = 5$ are shown in Fig. 6. Other parameters are: $p_0 = 250$ Pa, $T_0 = 250$ K, $T_w = 293$ K, $\gamma = 1.4$, and $R = 20$ mm. The shock wave moves downstream, strikes the sphere, and is reflected. Initially, this reflection is regular. When the angle of inclination of the incident shock to the surface has increased, Mach reflection occurs. Examples of regular and Mach reflection are shown in Fig. 6a for $\tau = 0.068$ (the dimensional time is $t = 1$ μs) and for $\tau = 0.4$ ($t = 5.9$ μs), respectively. However, this study did not particularly focus on the shock shape or shock position in detail; instead, transient pressure and heat flux at the stagnation point obtained by the above approximate solution and CFD are compared below.

Numerical simulations for the transient behavior of the shock detachment distance together with the theoretical results obtained by (6) are presented in Fig. 6b. The non-dimensional quantity ξ is plotted against the non-dimensional

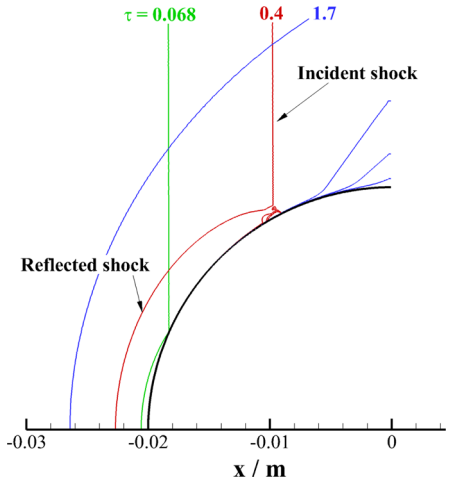

(a) Transient motion of the reflected shock by CFD

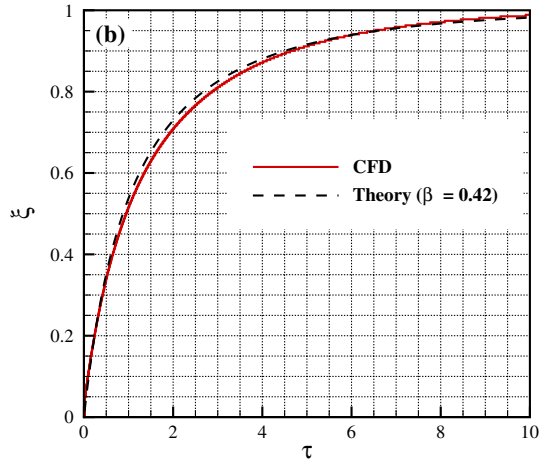

(b) Shock detachment histories

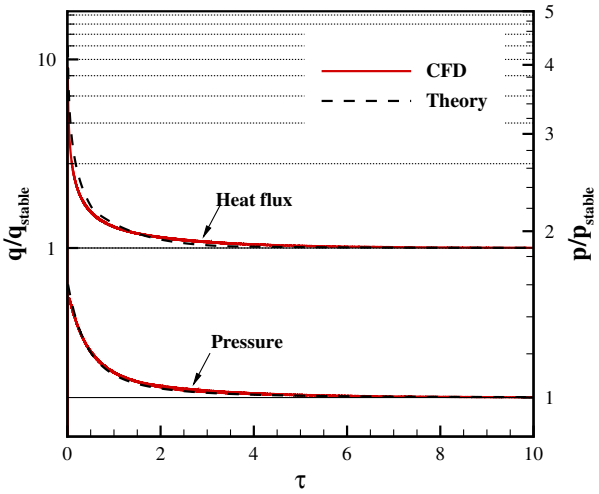

(c) Transient pressure and heat flux distributions

Fig. 6 Results for the diffraction of a normal shock wave over the sphere; $M_s = 5$, $p_0 = 250$ Pa, $T_0 = 250$ K, $T_w = 293$ K, $\gamma = 1.4$, and $R = 20$ mm

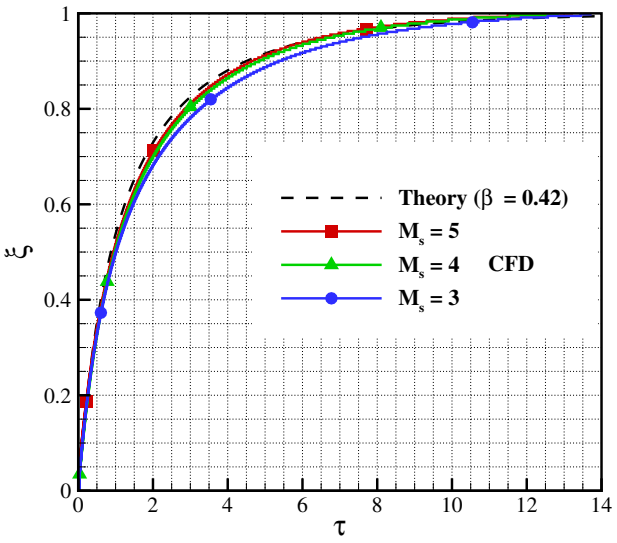

(a) Shock detachment histories

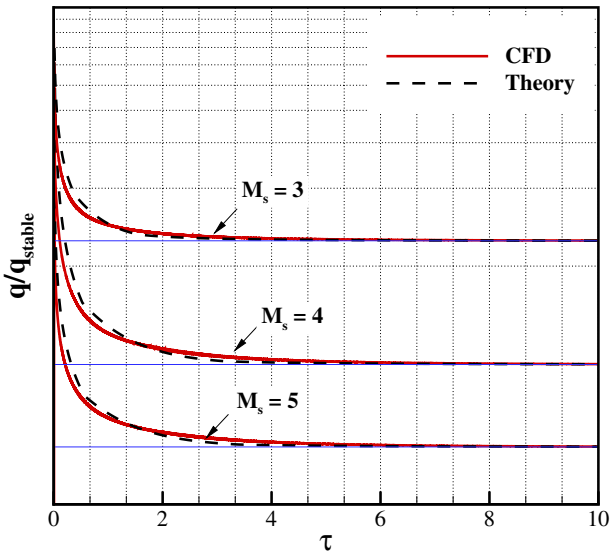

(b) Transient heat flux distributions

Fig. 7 Results of the diffraction of a normal shock wave over a sphere for different incident shock speeds; $p_0 = 250$ Pa, $T_0 = 250$ K, $T_w = 293$ K, $\gamma = 1.4$, and $R = 20$ mm

quantity τ, see (7). The analytical solution with $\beta = 0.42$ matches the numerical simulation well. Once the motion of the reflected shock is accurately obtained as a function of time, the transient parameters in region 3 and at the stagnation point (Fig. 1) can also be obtained; then, the transient pressure and heat flux during the detached bow shock establishment can be derived by the equations in Sect. 3. Their comparisons with the numerical results are shown in Fig. 6c. The theoretical pressure agrees well with the numerical pressure, which is not surprising since pressure is always relatively simple to simulate. As for the heat flux theoretical and numerical predictions, both also agree well for $\tau > 1$. However, con-

sidering the complexity of the prediction of aerodynamic heating [12], the difference between the theoretical and CFD simulation values for $\tau < 1$ may be also considered acceptable: The deviation is less than 15% most of the time. Thus, it may be concluded that the analytical equation (16) represents adequately the transient heat flux at the stagnation point during the establishment of the detached bow shock.

Moreover, pressure and heat flux at the stagnation point exceed considerably their steady-state values at the initial stage of reflection. Then, the pressure and heat flux drop rapidly and approach their steady-state values monotonically. A comparison of the results in Fig. 6b, c shows that the stagnation-point pressure and heat flux approach their steady values much more rapidly than the shock detachment distance does. The pressure is within about 5% of its final stable value at $\tau = 2$ ($t = 30$ μs), while the heat flux is within about 11% of its final value at this moment; however, at the same time the shock detachment distance has reached only about 70% of its final value. The shock detachment distance approaches 95% of its final value at $\tau \approx 6.5$ ($t \approx 96$ μs). Therefore, an estimate of the time required to establish steady or nearly steady values can be obtained from the above analysis.

To further validate the theoretical analyses of the present paper, different incident shock speeds were also investigated. The transient shock detachment and heat flux histories are shown in Fig. 7 for the incident shock Mach numbers varying from 3 to 5. A lower incident shock speed results in a larger difference between the theoretical and numerical results for shock detachment. However, the maximum difference is about 5% for $M_s = 3$ and less than 3% for $M_s = 4$ and 5. For the heat flux prediction, the analytical solutions show almost the same order of magnitude of the difference with the numerical values for all three cases. This suggests that they all match the numerical simulations well.

5 Conclusions

In the present study, numerical results are presented for the time histories of the shock detachment distance and the stagnation-point pressure and heat flux for a sphere which is washed by a normal shock wave. An analytical approach for the transient heat flux is also developed for an improved intuitive and accessible prediction; based on the theoretical description of the reflected shock position during bow shock formation, convective heat transfer is employed for a relatively long time after shock impingement by using the Fay and Riddell equation. The heat conduction between the stationary high-temperature gas and the cold wall is dominant at the initial stage, and a bridge function is constructed between the heat-conduction and convective-heat-transfer dominating periods. The approximate analytical solutions are validated by numerical simulations, and good agreement was obtained for the considered cases. The results provide an estimate of the necessary time to establish steady values. Furthermore, the stagnation-point pressure and heat flux approach their steady values much more rapidly than the shock detachment distance does. In summary, the present study is significant for understanding the heat transfer distributions during the detached bow shock establishment and helpful to provide guidance for the experimental design of aerodynamic-heating experiments in short-test-time impulsive facilities, such as shock tubes or expansion tubes.

Acknowledgements This work was supported by the National Natural Science Foundation of China (Grant Nos. 11402275, 11472280, and 11532014).

References

1. Mohammadiun, H., Rahimi, A.B.: Stagnation-point flow and heat transfer of a viscous, compressible fluid on a cylinder. J. Thermophys. Heat Transf. **26**, 494–502 (2012). https://doi.org/10.2514/1.T3833
2. Wang, Z.H., Bao, L., Tong, B.G.: Variation character of stagnation point heat flux for hypersonic pointed bodies from continuum to rarefied flow states and its bridge function study. Sci. China Ser. G **52**, 2007–2015 (2009). https://doi.org/10.1007/s11433-009-0226-7
3. Miles, J.W., Mirels, H., Wang, H.E.: Time required for establishing detached bow shock. AIAA J. **4**, 1127–1128 (1966). https://doi.org/10.2514/3.3633
4. Anderson, G.F.: Real gas effects on the time required for establishing a detached bow shock. AIAA J. **5**, 366–367 (1967). https://doi.org/10.2514/3.3981
5. Moran, J.P., Moorhem, W.K.: Diffraction of a plane shock by an analytic blunt body. J. Fluid Mech. **38**, 127–136 (1969). https://doi.org/10.1017/S0022112069000085
6. Barnwell, R.W.: Numerical results for the diffraction of a normal shock wave by a sphere and for the subsequent transient flow. NASA TR R-268 (1967)
7. Miller, C.G., Moore, J.A.: Flow-establishment times for blunt bodies in an expansion tube. AIAA J. **13**, 1676–1678 (1975). https://doi.org/10.2514/3.7048
8. Patz, G.: Formation of bow waves around blunt bodies in the flow behind a moving shock. Acta Mech. **32**, 89–100 (1979). https://doi.org/10.1007/BF01176136
9. Li, J.P., Chen, H., Zhang, S.Z., Zhang, X.Y., Yu, H.R.: On the response of coaxial surface thermocouples for transient aerodynamic heating measurements. Exp. Therm. Fluid Sci. **86**, 141–148 (2017). https://doi.org/10.1016/j.expthermflusci.2017.04.011
10. Collen, P.L., Doherty, L.J., McGilvray, M., Naved, I., Morgan, R.G., Hermann, D.E.: Commissioning of the T6 Stalker tunnel. AIAA Scitech 2019 Forum, San Diego, CA, AIAA Paper 2019-1941 (2019). https://doi.org/10.2514/6.2019-1941
11. Gildfind, D.E., James, C.M., Toniato, P., Morgan, R.G.: Performance considerations for expansion tube operation with a shock-heated secondary driver. J. Fluid Mech. **777**, 364–407 (2015). https://doi.org/10.1017/jfm.2015.349
12. McGilvray, M., Morgan, R.G., Jacobs, P.A.: Scramjet experiments in an expansion tunnel: evaluated using a quasi-steady analysis technique. AIAA J. **48**, 1635–1646 (2010). https://doi.org/10.2514/1.J050024

13. Candler, G.V., Subbareddy, P.K., Brock, J.M.: Advances in computational fluid dynamics methods for hypersonic flows. J. Spacecr. Rockets **52**, 17–28 (2015). https://doi.org/10.2514/1.A33023
14. Sun, Q.H., Zhu, H.Y., Wang, G., Fang, J.: Effects of mesh resolution on hypersonic heating prediction. Theor. Appl. Mech. Lett. **1**, 37–40 (2011). https://doi.org/10.1063/2.1102201
15. Li, X.D., Hu, Z.M., Jiang, Z.L.: Numerical investigation on the thermal protection mechanism for blunt body with forward-facing cavity. Sci. China Technol. Sci. **59**, 1–10 (2016). https://doi.org/10.1007/s11431-016-6015-4
16. Kim, K.H., Kim, C., Rho, O.H.: Methods for the accurate computations of hypersonic flows: I. AUSMPW+ scheme. J. Comput. Phys. **174**, 38–80 (2001). https://doi.org/10.1006/jcph.2001.6873
17. Kitamura, K., Shima, E., Nakamura, Y., Roe, P.L.: Evaluation of Euler flux for hypersonic heating computations. AIAA J. **48**, 763–776 (2001). https://doi.org/10.2514/1.41605
18. Jameson, A., Yoon, S.: Lower-upper implicit schemes with multiple grids for the Euler equations. AIAA J. **25**, 929–935 (1987). https://doi.org/10.2514/3.9724
19. Wang, Q., Li, J.P., Zhao, W., Jiang, Z.L.: Influence of thermal sensor installation on measuring accuracy at stagnation points. J. Thermophys. Heat Transf. **31**, 318–323 (2017). https://doi.org/10.2514/1.T4971
20. Billig, F.S.: Shock-wave shapes around spherical and cylindrical nosed bodies. J. Spacecr. Rockets **4**, 822–823 (1967). https://doi.org/10.2514/3.28969
21. Fay, J., Riddell, F.: Theory of stagnation point heat transfer in dissociated air. J. Aeronaut. Sci. **25**, 73–85 (1958). https://doi.org/10.2514/8.7517
22. Holman, J.P.: Heat Transfer, 10th edn. McGraw-Hill, New York (2010)
23. Wang, Q., Olivier, H., Einhoff, J., Li, J.P., Zhao, W.: Influence of test model material on the accuracy of transient heat transfer measurements in impulse facilities. Exp. Therm. Fluid Sci. **104**, 59–66 (2019). https://doi.org/10.1016/j.expthermflusci.2019.02.013